




OPEN The effect of critical coupling constants on superconductivity enhancement

Peir-Ru Wang , Jien-Wei Yeh & Yi-Hsien Lee

In this study, we propose a phenomenological model to extend McMillan's results on a coupling strength equal to 2. We investigate possible strategies to enhance superconductivity by tuning the phonon frequency, carrier number, or pressure. In particular, we show that the critical coupling constants corresponding to the phonon frequency, carrier number, or pressure determine whether the variation of the critical temperature is positive or negative. These observations explain the contrasting behavior between weak and strong coupling superconductors and are consistent with experimental observations. We also demonstrate the dome observed in the carrier number effect and pressure effect. Additionally, these critical coupling constants systematically separate superconductivity into three regions: weak, intermediate, and strong coupling. We find that the enhancement strategies for weak and strong coupling regions are opposite, but both inevitably bring superconductivity into the intermediate coupling region. Finally, we propose general zigzag methods for intermediate coupling superconductors to further enhance the critical temperature.

Notably, increasing the superconducting critical temperature T_c remains the principal problem of condensed matter physics since the discovery of superconductivity¹. Specifically, varying the phonon spectrum, tuning the carrier number, and increasing the pressure are three important experimental approaches to enhance T_c and consequently, speculate possible theories of superconductivity. However, the effects of altering these parameters on T_c are quite contrasting between weak coupling (low T_c) and strong coupling (high T_c) superconductivity. More precisely, first, in metallic superconductors^{2–6} and nickel-based superconductors⁷, which correspond to the case of weak coupling, the critical temperature T_c can be increased via phonon softening. In McMillan's results³, the maximum T_c appeared when the coupling strength is equal to 2. In contrast, in cuprate systems, which correspond to the case of strong coupling, T_c can be increased via phonon stiffening^{8,9}. Second, the effect of pressure on T_c is negative in most metallic superconductors^{10,11}. On the other hand, positive effects or a dome-like delineation appear in cuprate systems^{11,12}, iron-based^{13,14}, and hydrogen-rich superconductors^{15,16}. Third, in the phase diagrams that illustrate the variation of T_c with respect to the carrier number, the dome-like delineation may be observed in metallic^{17,18}, cuprates^{19–21}, and iron-based superconductors²². Specifically, the underdoped region is strongly coupled with a positive carrier number effect and becomes weakly coupled in the overdoped region with a negative carrier number effect²³. Besides, another approach to increase the carrier number is to gate thin film materials, which also demonstrates the dome-like effect^{24–26}. These three phenomena have a common dome-like delineation—the positive tendency appears in strong coupling superconductivity, and becomes negative in weak coupling superconductivity.

Furthermore, the T_c relation that derives from Cooper instability is a general property of superconductivity. Specifically, this relation may be written in the form $T_c \sim \mathcal{W} \exp(-\lambda^{-1})$ ^{2,27,28}, where \mathcal{W} is the bandwidth of superconducting electrons, and λ is the coupling constant of the pairing. Conventional superconductors, including metallic, MgB₂²⁹, and hydrogen-rich compounds, are adequately explained by phonon-mediated pairing^{2–4,16}. Meanwhile, unconventional superconductors, such as cuprates and iron-based superconductors are explained by Hubbard-type theories^{30–34}. Moreover, although the strong repulsion between electrons plays a major role in the Hubbard model, the electron–phonon interaction remains nonnegligible and consequently, contributes to the unconventional superconductivity^{21,35,36}. For this reason, in this study, we discuss the effects of varying the phonon spectrum, the carrier number, and the pressure on phonon-mediated pairing.

In the phonon-mediated pairing, the bandwidth \mathcal{W} is the characteristic phonon frequency Ω , and the coupling constant $\lambda = g(E_F) V_{eff}$ is the product of the effective interaction between electrons V_{eff} and the density of state at Fermi level $g(E_F)$. The effective interaction V_{eff} based on the Migdal theory³⁷ is $V_{eff} \sim 1/(M\Omega^2)$, and the density

Department of Materials Science and Engineering, National Tsing Hua University, 30013 Hsinchu, Taiwan. ✉email: louiscamry@gmail.com

of state at Fermi level³⁸ $g(\epsilon_F) = m^* \sqrt{3\pi^2 Z n_{ion}} / \pi^2 \hbar^2$, where M is the ion mass, m^* is the effective mass of an electron, Z is the valence number, and n_{ion} is the ion number density. Therefore, the explicit form of λ and T_c are

$$\lambda(\Omega) = \frac{C \sqrt[3]{Z n_{ion}}}{M \Omega^2} \quad (1)$$

and

$$T_c(\Omega) \sim \Omega \exp \left[-\frac{M \Omega^2}{C \sqrt[3]{Z n_{ion}}} \right], \quad (2)$$

where C is a constant. Notice that Eq. (1) is similar to McMillan³. However, we preserve the term $\sqrt[3]{Z n_{ion}}$ to describe the carrier number effect and the pressure effect. First, to investigate the phonon effect on superconductivity, the derivative of Eqs. (1) and (2) with respect to Ω are

$$\frac{d\lambda}{d\Omega} = -2 \frac{\lambda}{\Omega} \quad (3)$$

and

$$\frac{dT_c}{d\Omega} = \frac{T_c}{\Omega} \left(1 - \frac{2}{\lambda} \right). \quad (4)$$

The derivative $dT_c/d\Omega$ is equal to 0 when λ is equal to 2. Define the critical coupling constant corresponding to the phonon frequency $\lambda_c^{\Omega}=2$.

Second, to investigate the dependency of λ and T_c on carrier number Z , Eqs. (1) and (2) can be rewritten as a function of the carrier number Z . Here, the characteristic phonon frequency Ω uses the jellium phonon frequency³⁹ $\Omega = \sqrt{Z^2 e^2 n_{ion} / \epsilon_0 M}$, where ϵ_0 is the permittivity. The explicit form of λ and T_c as a function of Z are

$$\lambda(Z) = \frac{C \epsilon_0}{e^2 n_{ion}^{2/3}} Z^{-5/3} \quad (5)$$

and

$$T_c(Z) \sim \left(\frac{Z^2 e^2 n_{ion}}{\epsilon_0 M} \right)^{1/2} \exp \left(-\frac{C \epsilon_0}{e^2 n_{ion}^{2/3}} Z^{-5/3} \right). \quad (6)$$

The derivative of Eqs. (5) and (6) with respect to Z are

$$\frac{d\lambda}{dZ} = -\frac{5}{3} \frac{\lambda}{Z} \quad (7)$$

and

$$\frac{dT_c}{dZ} = \frac{T_c}{Z} \left[1 - \left(\frac{5}{3} \right) \frac{1}{\lambda} \right]. \quad (8)$$

Similarly, the derivative dT_c/dZ is equal to 0 when λ is equal to 5/3, denoted as λ_c^Z .

Third, to investigate the dependency of T_c on pressure P , the compressibility $\beta = -(1/V) * (dV/dP)$ can be adopted to relate the pressure P and the volume V . Using $n_{ion} = N_{ion}/V$, where N_{ion} is the number of ions; Eqs. (5) and (6) can thus be rewritten into a function of V :

$$\lambda(V) = \frac{C \epsilon_0}{e^2 Z^{5/3} N_{ion}^{2/3}} V^{2/3} \quad (9)$$

and

$$T_c(V) \sim \left(\frac{Z^2 e^2 N_{ion}}{\epsilon_0 M V} \right)^{1/2} \exp \left(-\frac{e^2 Z^{5/3} N_{ion}^{2/3}}{C \epsilon_0} V^{-2/3} \right). \quad (10)$$

The derivative of Eqs. (9) and (10) with respect to the pressure P are:

$$\frac{d\lambda}{dP} = \frac{dV}{dP} * \frac{d\lambda}{dV} = -\beta V * \frac{2}{3} \frac{\lambda}{V} \quad (11)$$

and

$$\frac{dT_c}{dP} = \frac{dV}{dP} * \frac{dT_c}{dV} = \beta V * \frac{1}{2} \frac{T_c}{V} \left[1 - \left(\frac{4}{3} \right) \frac{1}{\lambda} \right]. \quad (12)$$

The critical coupling constant corresponding to the pressure is $\lambda_c^P=4/3$. The schematic diagram based on the result from Eqs. (1) to (12), which demonstrates the effects of tuning Ω , Z , or P on T_c is plotted in Fig. 1.

Results and discussion

The origin of the dome. The results of our derivations reveal two common features: (1) $dT_c/d\mathcal{X} \propto 1 - (\lambda_c^{\mathcal{X}}/\lambda)$, and (2) $d\lambda/d\mathcal{X} < 0$, where \mathcal{X} represents Ω , Z , or P . Specifically, feature (1) indicates that there is a sign change of derivative $d\lambda/d\mathcal{X}$ at $\lambda_c^{\mathcal{X}}$. If λ is larger than $\lambda_c^{\mathcal{X}}$, the effect of varying \mathcal{X} on superconductivity is positive with T_c increasing, which corresponds to strong coupling superconductivity. On the other hand, if λ is smaller than $\lambda_c^{\mathcal{X}}$, then the effect of varying \mathcal{X} on superconductivity is negative with T_c decreasing, which corresponds to weak coupling superconductivity. These observations explain the contrasting behavior between weak and strong coupling superconductors. Feature (2) is the reason for the dome-like delineation observed in many strong coupling superconductors. Specifically, for strong coupling superconductors, the coupling constant is expected to be larger than $\lambda_c^{\mathcal{X}}$, to ensure the effect of varying \mathcal{X} on superconductivity is positive. In addition, since the derivative of λ is negative, λ decreases when the parameter \mathcal{X} increases. In particular, once λ becomes smaller than $\lambda_c^{\mathcal{X}}$, the effect of varying \mathcal{X} on superconductivity becomes negative. This transition from positive to negative demonstrates the dome-like delineation and can be observed when tuning the carrier number or varying the pressure in the experiments.

Critical temperature T_c as a function of phonon frequency Ω . Critical temperature T_c is influenced when the phonon frequency Ω is changing. Specifically, the maximum T_c appears at $\lambda_c^\Omega = 2$ by varying the phonon frequency Ω , which is consistent with McMillan³. More precisely, in the $\lambda > \lambda_c^\Omega$ region, the sign of $dT_c/d\Omega$ is positive, and T_c increases when increasing Ω . This region may correspond to cuprate superconductors. Particularly, LaBaCuO, YBaCuO, BiSrCaCuO, HgBaCaCuO, and TlBaCaCuO demonstrate phonon stiffening effect^{8,9}. In Table 1, the λ value of phonon stiffening effect superconductors are listed. For example, the value of the coupling constant λ at optimal T_c of Bi₂Sr₂Ca₀Cu₁O_x, Bi₂Sr₂Ca₁Cu₂O_x, and Bi₂Sr₂Ca₂Cu₃O_x are 2.95, 2.15, and 2.18, respectively²¹. These λ values are larger than λ_c^Ω indicating that T_c can be enhanced by the phonon stiffening effect.

Meanwhile, in the $\lambda < \lambda_c^\Omega$ region, the coupling constant λ is smaller than λ_c^Ω . Specifically, the sign of $dT_c/d\Omega$ is negative and T_c decreases when Ω increases. More precisely, this region may correspond to traditional metallic superconductors. Particularly, VCr, ZrRh, NbMo, MoRe, WRe, PbTl, PbBi, Nb₃Al, and Nb₃Ge demonstrate the phonon softening effect^{3–6}. In Table 1, the λ value of phonon softening effect superconductors are listed. For example, when the Debye temperature Θ_D of the VCr alloy increases from 370 to 470 K, T_c decreases from 3.21 to 0.10 K, and λ decreases from 0.53 to 0.33. Taking another example, when the Debye temperature Θ_D of the ZrRh alloy increases from 192 to 244 K, T_c decreases from 5.95 to 3.10 K, and λ decreases from 0.80 to 0.59. The experiment data show that the coupling constant λ decreases when the phonon frequency increases, which is consistent with our result $d\lambda/d\Omega < 0$ from Eq. (3). A similar effect also appears in nickel-based superconductors⁷, which validates that the superconductivity is enhanced by giant phonon softening.

Critical temperature T_c as a function of carrier number Z . The effect of carrier number on superconductivity through varying the alloy composition, doping concentration, or gating voltage has been widely studied

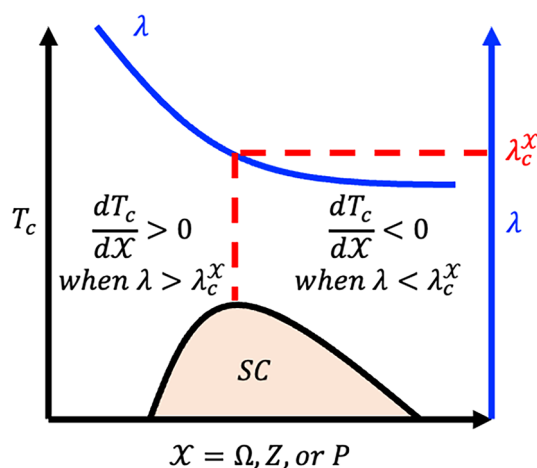


Figure 1. A schematic diagram of the critical temperature T_c and the critical coupling constants $\lambda_c^{\mathcal{X}}$ corresponding to the phonon frequency Ω , the carrier number Z , and the pressure P . There is a sign change of derivative $d\lambda/d\mathcal{X}$ at $\lambda_c^{\mathcal{X}}$. If λ is larger than $\lambda_c^{\mathcal{X}}$, the effect of varying \mathcal{X} on superconductivity is positive with T_c increasing corresponding to strong coupling superconductivity. Meanwhile, if λ is smaller than $\lambda_c^{\mathcal{X}}$, then the effect of varying \mathcal{X} on superconductivity is negative with T_c decreasing corresponding to the weak coupling superconductivity.

Compound	λ
Phonon stiffening	
$\text{Bi}_2\text{Sr}_2\text{Ca}_0\text{Cu}_1\text{O}_x$	2.95 ²¹
$\text{Bi}_2\text{Sr}_2\text{Ca}_1\text{Cu}_2\text{O}_x$	2.15 ²¹
$\text{Bi}_2\text{Sr}_2\text{Ca}_2\text{Cu}_3\text{O}_x$	2.18 ²¹
$\text{YBa}_2\text{Cu}_3\text{O}_x$	2.32 ⁴⁰
Phonon softening	
VCr	0.53 ³
ZrRh	0.80 ³
NbMo	0.7 ³
MoRe	0.86 ³
WRe	0.60 ³
PbTl	1.53 ⁴
PbBi	1.66 ⁴
Nb_3Al	1.2–1.82 ^{5,41}
Nb_3Ge	0.7–1.5 ⁶
BaNi_2As_2	0.16–0.24 ⁴²

Table 1. Examples of phonon effect Ω on superconductivity and λ value. The critical coupling constant corresponding to the phonon frequency is $\lambda_c^\Omega = 2$. The phonon stiffening effect appears when $\lambda > \lambda_c^\Omega$, and the phonon softening effect appears when $\lambda < \lambda_c^\Omega$.

in material physics. Particularly, the dome-like delineation was observed in metallic materials¹⁷, cuprates^{19–21}, iron-based systems²², and gating thin film materials²⁴. More precisely, the maximum T_c appears at $\lambda_c^Z = 5/3$ by varying the carrier number Z .

For conventional superconductors, we take $\text{Nb}_3\text{Al}_{1-x}\text{Ge}_x$ as an example⁴³, which is showing in Fig. 2a. Specifically, when the Ge component rises from $x=0$ to $x=0.29$, the electrons per atom ratio (e/a) rises from 4.50 to 4.57 and T_c increases from 18 to 21 K. The coupling constant of Nb_3Al_1 is $\lambda > 1.8$ ⁴¹, which is greater than λ_c^Z and

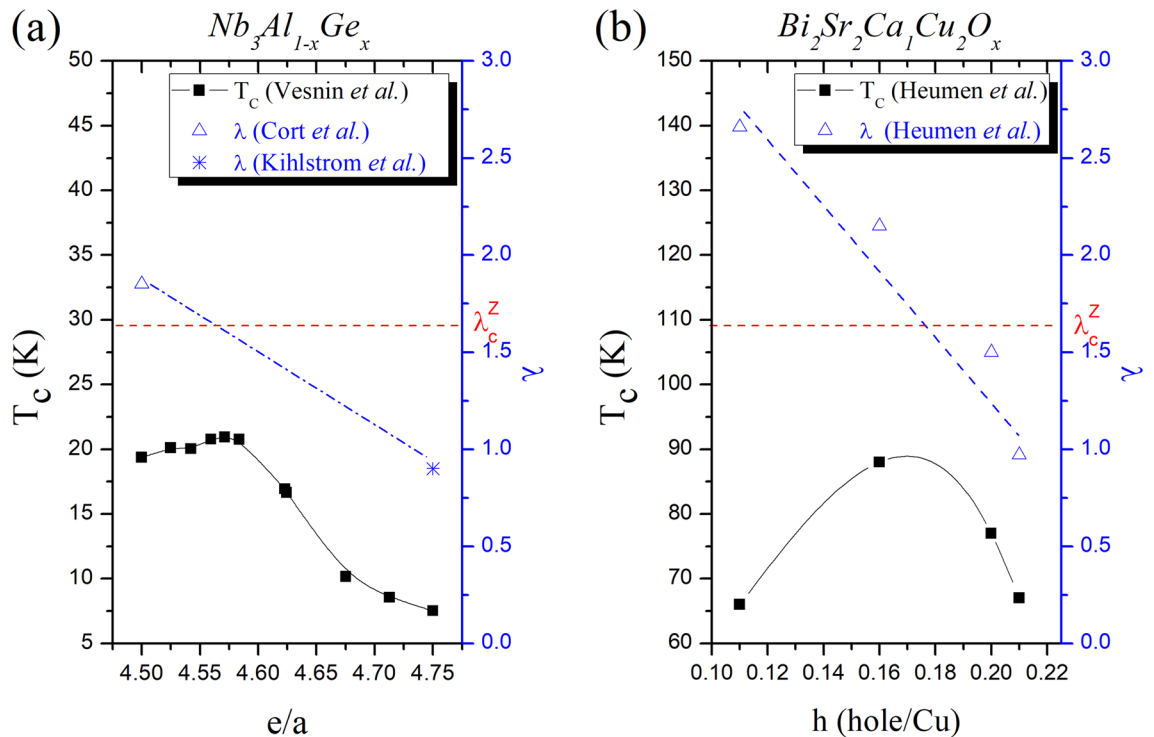


Figure 2. Examples of carrier number effect Z on superconductivity. (a) The conventional superconductors $\text{Nb}_3\text{Al}_{1-x}\text{Ge}_x$ demonstrates carrier effect^{5,6,41,43}. Specifically, the electrons per atom ratio (e/a) rises from 4.50 to 4.75 and T_c shows dome-like effect. (b) The hole-doped h (holes/Cu) experiment of the unconventional superconductors $\text{Bi}_2\text{Sr}_2\text{Ca}_1\text{Cu}_2\text{O}_x$ demonstrates dome-like effect²¹. The critical coupling constant corresponding to Z is $\lambda_c^Z = 5/3$. Both cases show that T_c is increasing when $\lambda > \lambda_c^Z$, and T_c is decreasing when $\lambda < \lambda_c^Z$.

is consistent with the positive carrier effect. Moreover, when the Ge component rises from $x=0.29$ to $x=1$, the e/a ratio rises from 4.57 to 4.75 and T_c decreases from 21 to 7 K. The coupling constant of Nb_3Ge_1 is $\lambda < 1$ ⁶ which is smaller than λ_c^Z and is consistent with the negative carrier effect.

For unconventional superconductors, we take the hole-doped experiment of $\text{Bi}_2\text{Sr}_2\text{Ca}_1\text{Cu}_2\text{O}_x$ as an example²¹, which is showing in Fig. 2b. Specifically, when the hole doping h (holes/Cu) rises from $h=0.11$ to $h=0.21$, the coupling constant monotonically decreases from $\lambda = 2.66$ to $\lambda = 0.97$. Additionally, the critical temperature first rises from 66 K ($\lambda = 2.66 > \lambda_c^Z$ at $h=0.11$) to 88 K ($\lambda = 2.15 > \lambda_c^Z$ at $h=0.16$), then drops to 77 K ($\lambda = 1.5 < \lambda_c^Z$ at $h=0.20$) and further to 67 K ($\lambda = 0.97 < \lambda_c^Z$ at $h=0.21$). This dome-like delineation showed that the superconductivity is increasing in the underdoped region with coupling λ stronger than λ_c^Z , and decreasing in the overdoped region with coupling λ weaker than λ_c^Z .

Critical temperature T_c as a function of pressure effect P . The effect of pressure on superconductivity is an important topic in the field of condensed matter physics. In particular, for strong coupling superconductors, the pressure effect is positive and may lead to a dome-like delineation at higher pressure. These characteristics were observed in cuprate superconductors^{12,44}, iron-based superconductors^{13,14,45}, and hydrogen-rich superconductors^{15,16}. In Table 2, the λ value of positive or dome-like pressure effect superconductors are listed. Specifically, the coupling constants of cuprates are greater than λ_c^P as mentioned in the previous section. Here, we note the couple constant of iron-based superconductors; for instance, $\text{LaFeAsO}_{1-x}\text{F}_x$ and $\text{Ba}(\text{Fe}_{1-x}\text{Co}_x)_2\text{As}_2$ are $\lambda = 2.38$ and 2.83, respectively⁴⁶. These strong coupling superconductors have coupling strength λ larger than λ_c^P , thus the positive or dome-like delineation of the pressure effect can be observed.

Meanwhile, most metallic superconductors are weak-coupling superconductors. Particularly, Al, Cd, Sn, In, and Pb are examples with negative pressure effect^{10,11}. Specifically, the coupling constant λ of Al, Cd, Sn, In, and Pb are less than λ_c^P (see Table 2). Clearly, these superconductors have λ less than λ_c^P . Additionally, the negative pressure effect is also observed in the covalent compound MgB_2 ¹¹, with λ equal to 0.7⁴⁹, which is smaller than λ_c^P .

The strategies of T_c enhancement. According to these three critical coupling constants: λ_c^Ω , λ_c^Z , and λ_c^P , superconductors can be classified by their coupling strength: weak coupling ($\lambda < \lambda_c^P$), intermediate coupling ($\lambda_c^P < \lambda < \lambda_c^\Omega$), and strong coupling ($\lambda > \lambda_c^\Omega$). A schematic diagram can be seen in Fig. 3.

In the weak coupling region ($\lambda < \lambda_c^P$), the coupling constant λ is less than λ_c^P . Particularly, all derivatives of critical temperature $dT_c/d\Omega$, dT_c/dZ , and dT_c/dP are negative, as shown in Fig. 3. Hence, by decreasing Ω , Z or P , the superconductivity can be enhanced. These procedures increase the coupling constant λ , because the derivatives of the coupling constant $d\lambda/d\Omega$, $d\lambda/dZ$, and $d\lambda/dP$ are negative. We can accurately infer that the superconductivity of weak coupling superconductors is enhanced by increasing the coupling strength. In addition, once the coupling constant λ becomes greater than λ_c^P , the superconductivity enters into the intermediate region, and the tendencies of T_c become complicated.

Meanwhile, in the strong coupling region ($\lambda > \lambda_c^\Omega$), the coupling constant λ is larger than λ_c^Ω . Particularly, all derivatives of the critical temperature $dT_c/d\Omega$, dT_c/dZ , and dT_c/dP are positive in Fig. 3, thus the superconductivity can be increased by increasing Ω , Z or P . These procedures decrease the coupling constant λ , such that we can adequately infer that the superconductivity of strong coupling superconductors is enhanced by decreasing the coupling strength. Once the coupling constant λ is smaller than λ_c^Ω , the superconductivity enters into the intermediate coupling region and the tendencies of T_c become complicated. Besides, comparing the strong coupling region with the weak coupling region, three tendencies of T_c are contrasting between the two regions.

Compound	λ
Positive or dome-like	
$\text{Bi}_2\text{Sr}_2\text{Ca}_0\text{Cu}_1\text{O}_x$	2.95 ²¹
$\text{YBa}_2\text{Cu}_3\text{O}_x$	2.32 ⁴⁰
$\text{LaFeAsO}_{1-x}\text{F}_x$	2.38 ⁴⁶
$\text{Ba}(\text{Fe}_{1-x}\text{Co}_x)_2\text{As}_2$	2.83 ⁴⁶
FeSe	1.6 ⁴⁷
H_2S	~ 2 ⁴⁸
Negative	
Al	0.38 ³
Cd	0.38 ³
Sn	0.6 ³
In	0.69 ³
Pb	1.12 ³
MgB_2	0.7 ⁴⁹

Table 2. Examples of pressure effect P on superconductivity and λ value. The critical coupling constant corresponding to the pressure is $\lambda_c^P = 4/3$. The positive or dome-like pressure effect appears when $\lambda > \lambda_c^P$, and the negative pressure effect appears when $\lambda < \lambda_c^P$.

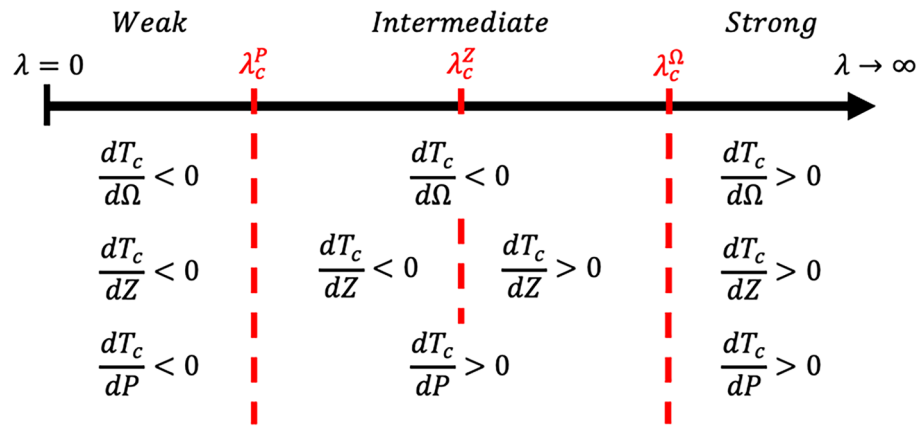


Figure 3. Classification and enhancement strategy for superconductivity. Using three critical coupling constants: λ_c^Ω , λ_c^Z , and λ_c^P , superconductors can be classified by their coupling strength: weak coupling ($\lambda < \lambda_c^P$), intermediate coupling ($\lambda_c^P < \lambda < \lambda_c^\Omega$), and strong coupling ($\lambda > \lambda_c^\Omega$).

Moreover, in the intermediate coupling region ($\lambda_c^P < \lambda < \lambda_c^\Omega$), the enhancement methods are more interesting. In particular, take that λ belongs in the interval $\lambda_c^P < \lambda < \lambda_c^Z$ for the following discussion without loss of generality. In this interval, superconductivity can be enhanced by increasing P or decreasing Z . First, let the superconductivity be optimized by tuning Z , such that λ is equal to λ_c^Z , denoted as λ_1 . Second, since λ_1 is larger than λ_c^P , we can increase P to increase T_c . The second step causes λ to decrease and T_c is optimized when $\lambda = \lambda_c^P$, denoted as λ_2 . Third, now λ_2 is smaller than λ_c^Z , T_c can be further increased by decreasing Z . The third step increases λ and T_c is optimized when $\lambda = \lambda_c^Z$, denoted as λ_3 . Repeat step 2 and step 3 by increasing P and decreasing Z alternately; T_c can be enhanced like a zigzag mountain climbing. In this study, we propose simultaneously gating and pressurizing on thin-film superconductors to verify our discussion. Furthermore, FeSe has been observed under gating²⁵ and pressurizing⁵⁰ independently. More precisely, the negative carrier number effect and the dome-like pressure effect suggest the coupling strength $\lambda_c^P < \lambda_{\text{FeSe}} < \lambda_c^Z$, which agree with $\lambda_{\text{FeSe}} = 1.6$ ⁴⁷. Additionally, we propose that increasing P and decreasing Ω alternately, or increasing Z and decreasing Ω alternately, are two other methods to enhance superconductivity in the intermediate region.

Conclusion

In this study, we proposed a phenomenological model based on phonon-mediated interaction, which explains the difference between weak and strong coupling superconductors affected by tuning phonon frequency Ω , carrier number Z , and pressure P . We introduced the concept of critical coupling constants and enhancement strategies for superconductivity, extending McMillan's results on coupling strength equal to 2. Specifically, the sign of the first-order derivative $dT_c/d\mathcal{X}$ with respect to $\mathcal{X} = \Omega, Z, \text{ or } P$, indicates that T_c is increasing or decreasing when either these three parameters change. More precisely, these three derivatives have two features in common: (1) the coupling constant λ beyond (or below) the critical coupling constant $\lambda_c^\mathcal{X}$ determined $dT_c/d\mathcal{X}$ to be positive (or negative), and (2) the dome-like delineation observed in strong coupling superconductors because $d\lambda/d\mathcal{X}$ is always negative. Overall, these observations explain the differences between weak and strong superconductors.

Furthermore, using three critical coupling constants λ_c^Ω , λ_c^Z , and λ_c^P , superconductors can be classified by their coupling strength and consequently, correspond to different enhancement strategies. Specifically, for the weak coupling region ($\lambda < \lambda_c^P$), T_c can be increased by decreasing Ω , Z , and P , causing λ to be increased, resulting in intermediate coupling. In contrast, superconductors in the strong coupling region ($\lambda > \lambda_c^\Omega$) can be enhanced by increasing Ω , Z , and P , causing λ to be decreased, resulting in intermediate coupling. Moreover, for superconductors in the intermediate coupling region ($\lambda_c^P < \lambda < \lambda_c^\Omega$), the zigzag strategies may further enhance superconductivity.

Data availability

The datasets used and analyzed during the current study are available from the corresponding author on reasonable request.

Received: 2 March 2023; Accepted: 19 April 2023

Published online: 20 April 2023

References

- Onnes, H. K. Investigations into the properties of substances at low temperatures, which have led, amongst other things, to the preparation of liquid helium. *Nobel Lect.* **4**, 306–336 (1913).
- Bardeen, J., Cooper, L. N. & Schrieffer, J. R. Theory of superconductivity. *Phys. Rev.* **108**, 1175 (1957).
- McMillan, W. L. Transition temperature of strong-coupled superconductors. *Phys. Rev.* **167**, 331–344 (1968).
- Allen, P. B. & Dynes, R. Transition temperature of strong-coupled superconductors reanalyzed. *Phys. Rev. B* **12**, 905 (1975).
- Kwo, J. & Geballe, T. Superconducting tunneling into the A_{15} Nb_3Al thin films. *Phys. Rev. B* **23**, 3230 (1981).
- Kihlstrom, K. & Geballe, T. Tunneling $\alpha^2F(\omega)$ as a function of composition in A_{15} NbGe . *Phys. Rev. B* **24**, 4101 (1981).

7. Kudo, K., Takasuga, M., Okamoto, Y., Hiroi, Z. & Nohara, M. Giant phonon softening and enhancement of superconductivity by phosphorus doping of BaNi₂As₂. *Phys. Rev. Lett.* **109**, 097002 (2012).
8. Ledbetter, H., Kim, S. & Roshko, A. Critical-temperature/Debye-temperature correlation in (La-M)₂CuO₄ superconductors. *Phys. C Supercond.* **190**, 129–130 (1991).
9. Ledbetter, H. Dependence of T_c on Debye temperature Θ_D for various cuprates. *Phys. C Supercond.* **235**, 1325–1326 (1994).
10. Smith, T. & Chu, C. Will pressure destroy superconductivity?. *Phys. Rev.* **159**, 353 (1967).
11. Lorenz, B. & Chu, C. *Frontiers in Superconducting Materials* 459–497 (Springer, 2005).
12. Sadewasser, S., Schilling, J., Paulikas, A. & Veal, B. Pressure dependence of T_c to 17 GPa with and without relaxation effects in superconducting YBa₂Cu₃O_x. *Phys. Rev. B* **61**, 741 (2000).
13. Sefat, A. S. Pressure effects on two superconducting iron-based families. *Rep. Prog. Phys.* **74**, 124502 (2011).
14. Sang, L. *et al.* Pressure effects on iron-based superconductor families: Superconductivity, flux pinning and vortex dynamics. *Mater. Today Phys.* **19**, 100414 (2021).
15. Drozdov, A., Erements, M., Troyan, I., Ksenofontov, V. & Shylin, S. I. Conventional superconductivity at 203 kelvin at high pressures in the sulfur hydride system. *Nature* **525**, 73–76 (2015).
16. Drozdov, A. *et al.* Superconductivity at 250 K in lanthanum hydride under high pressures. *Nature* **569**, 528–531 (2019).
17. Matthias, B. T. Empirical relation between superconductivity and the number of valence electrons per atom. *Phys. Rev.* **97**, 74 (1955).
18. Yeh, J. W. *et al.* Nanostructured high-entropy alloys with multiple principal elements: Novel alloy design concepts and outcomes. *Adv. Eng. Mater.* **6**, 299–303 (2004).
19. Charnukha, A. Optical conductivity of iron-based superconductors. *J. Phys. Condens. Matter.* **26**, 253203 (2014).
20. Lee, P. A., Nagaosa, N. & Wen, X.-G. Doping a Mott insulator: Physics of high-temperature superconductivity. *Rev. Mod. Phys.* **78**, 17 (2006).
21. Van Heumen, E. *et al.* Optical determination of the relation between the electron-boson coupling function and the critical temperature in high-T_c cuprates. *Phys. Rev. B* **79**, 184512 (2009).
22. Aoki, H. & Hosono, H. A superconducting surprise comes of age. *Phys. World* **28**, 31 (2015).
23. Sleight, A. W. Room temperature superconductors. *Acc. Chem. Res.* **28**, 103–108 (1995).
24. Shi, W. *et al.* Superconductivity series in transition metal dichalcogenides by ionic gating. *Sci. Rep.* **5**, 1–10 (2015).
25. Lei, B. *et al.* Evolution of high-temperature superconductivity from a low-T_c phase tuned by carrier concentration in FeSe thin flakes. *Phys. Rev. Lett.* **116**, 077002 (2016).
26. Liu, X. *et al.* Nonlinear valley phonon scattering under the strong coupling regime. *Nat. Mater.* **20**, 1210–1215 (2021).
27. Hirsch, J. E. Two-dimensional Hubbard model: Numerical simulation study. *Phys. Rev. B* **31**, 4403 (1985).
28. Raghu, S., Kivelson, S. & Scalapino, D. Superconductivity in the repulsive Hubbard model: An asymptotically exact weak-coupling solution. *Phys. Rev. B* **81**, 224505 (2010).
29. Moshchalkov, V. *et al.* Type-1.5 Superconductivity. *Phys. Rev. Lett.* **102**, 117001 (2009).
30. Anderson, P. W. The resonating valence bond state in La₂CuO₄ and superconductivity. *Science* **235**, 1196–1198 (1987).
31. Schrieffer, J., Wen, X.-G. & Zhang, S.-C. Spin-bag mechanism of high-temperature superconductivity. *Phys. Rev. Lett.* **60**, 944 (1988).
32. Monthoux, P. & Lonzarich, G. p-wave and d-wave superconductivity in quasi-two-dimensional metals. *Phys. Rev. B* **59**, 14598 (1999).
33. Laad, M. S. & Craco, L. Theory of multiband superconductivity in iron pnictides. *Phys. Rev. Lett.* **103**, 017002 (2009).
34. Laussy, F. P., Kavokin, A. V. & Shelykh, I. A. Exciton-polariton mediated superconductivity. *Phys. Rev. Lett.* **104**, 106402 (2010).
35. Zhao, G.-M., Keller, H. & Conder, K. Unconventional isotope effects in the high-temperature cuprate superconductors. *J. Phys. Condens. Matter.* **13**, R569 (2001).
36. Zhang, C. *et al.* Ubiquitous strong electron-phonon coupling at the interface of FeSe/SrTiO₃. *Nat. Commun.* **8**, 1–6 (2017).
37. Annett, J. F. *Superconductivity, Superfluids and Condensates* Vol. 5 (Oxford University Press, 2004).
38. Kittel, C. *Solid State Physics* Vol. 3 (Shell Development Company, 1955).
39. Bruus, H. & Flensberg, K. *Many-Body Quantum Theory in Condensed Matter Physics: An Introduction* (OUP, 2004).
40. Ledbetter, H., Lei, M. & Kim, S. Elastic constants, Debye temperatures, and electron-phonon parameters of superconducting cuprates and related oxides. *Phase Transit.* **23**, 61–70 (1990).
41. Cort, B., Stewart, G., Snead, C. Jr., Sweedler, A. & Moehlecke, S. Specific-heat studies of neutron-irradiated A15 Nb₃Al. *Phys. Rev. B* **24**, 3794 (1981).
42. Shein, I. R. & Ivanovskii, A. L. Electronic and structural properties of low-temperature superconductors and ternary pnictides ANi₂Pn₂ (A = Sr, Ba and Pn = P, As). *Phys. Rev. B* **79**, 054510 (2009).
43. Vesnin, Y. I., Eltsev, Y. F., Zakovryashin, S. & Starikov, M. Superconductivity and decay Phenomena of Nb₃Al-Nb₃Ge solid solutions. *Phys. Status Solidi (a)* **77**, 759–764 (1983).
44. Chu, C. Superconductivity at higher temperatures in the Hg-Ba-Ca-Cu-O compound system. *J. Supercond.* **7**, 1–7 (1994).
45. Liu, W. *et al.* Pressure-tuned superconductivity and normal-state behavior in Ba(Fe_{0.943}Co_{0.057})₂As₂ near the antiferromagnetic boundary. *Phys. Rev. B* **97**, 144515 (2018).
46. Ummarino, G. Multiband s± Eliashberg theory and temperature-dependent spin-resonance energy in iron pnictide superconductors. *Phys. Rev. B* **83**, 092508 (2011).
47. Coh, S., Cohen, M. L. & Louie, S. G. Large electron-phonon interactions from FeSe phonons in a monolayer. *New J. Phys.* **17**, 073027 (2015).
48. Mozaffari, S. *et al.* Superconducting phase diagram of H₃S under high magnetic fields. *Nat. Commun.* **10**, 2522 (2019).
49. Kortus, J., Mazin, I., Belashchenko, K. D., Antropov, V. P. & Boyer, L. Superconductivity of metallic boron in MgB₂. *Phys. Rev. Lett.* **86**, 4656 (2001).
50. Deng, L. *et al.* Pressure-induced high-temperature superconductivity retained without pressure in FeSe single crystals. *Proc. Natl. Acad. Sci. USA.* **118**, e2108938118 (2021).

Acknowledgements

The authors thank C.-Y. Mou, P.-Y. Chang, K.-A. Wu, C.-L. Wang, and K.-H. Lin for their helpful discussions. In memory of T.-Y. Liu.

Author contributions

P.-R.W. contributed to the theory and analysis. J.-W.Y. and Y.-H.L. contributed to the discussion on the interpretation of the theory. All authors contributed to the preparation and revision of the manuscript.

Competing interests

The authors declare no competing interests.

Additional information

Correspondence and requests for materials should be addressed to P.-R.W.

Reprints and permissions information is available at www.nature.com/reprints.

Publisher's note Springer Nature remains neutral with regard to jurisdictional claims in published maps and institutional affiliations.



Open Access This article is licensed under a Creative Commons Attribution 4.0 International License, which permits use, sharing, adaptation, distribution and reproduction in any medium or format, as long as you give appropriate credit to the original author(s) and the source, provide a link to the Creative Commons licence, and indicate if changes were made. The images or other third party material in this article are included in the article's Creative Commons licence, unless indicated otherwise in a credit line to the material. If material is not included in the article's Creative Commons licence and your intended use is not permitted by statutory regulation or exceeds the permitted use, you will need to obtain permission directly from the copyright holder. To view a copy of this licence, visit <http://creativecommons.org/licenses/by/4.0/>.

© The Author(s) 2023